RESEARCH ARTICLE

physica status solidi b

www.pss-b.com

Check for updates

Selective Area Growth of Cubic Gallium Nitride in Nanoscopic Silicon Dioxide Masks

Falco Meier, Mario Littmann, Julius Bürger, Thomas Riedl, Daniel Kool, Jörg Lindner, Dirk Reuter, and Donat Josef As**

Herein, the possibilities of nanoselective area growth (NSAG) of cubic gallium nitride on 3C-SiC/Si (001) pseudo substrates are studied. Growth is masked by SiO_2 patterned with hole arrays and groove structures. Nanosphere lithography and block-copolymer lithography are employed to pattern holes with diameters of 130 and 17 nm, respectively. Electron beam lithography is used to pattern grooves. Patterns are transferred into SiO_2 and 3C-SiC by reactive ion etching with CHF_3/Ar and SF_6 chemistry, correspondingly. It is possible to demonstrate phase pure nanoselective nucleation of c-GaN on <001> and <111> facets of 3C-SiC. Phase pure nucleation of cubic gallium nitride is confirmed by transmission electron microscopy measurements on the nanoscopic scale. A hexagonal fraction of 17.6% is achieved on the macroscopic scale measured by high-resolution X-ray diffraction (HRXRD), employing V-shaped grooves on 4° miscut substrates. Furthermore, the possibility of coalescence after NSAG is demonstrated with the dominant cubic phase.

1. Introduction

Research for group III nitrides usually refers to the hexagonal wurtzite phase. Nevertheless, it is also possible to grow nitrides in the cubic phase. Besides the favorable mechanical,[1] thermal,[1,2] and electro-optical[1,3] properties of nitrides, the efficiency of devices is considerably diminished by the quantum confined Stark effect (QSCE).[1] QSCE is a result of polarization fields introduced by the crystal symmetry of a wurtzite unit cell based on different atoms.[4] Despite more contributions to the internal quantum efficiency of devices made of hexagonal group III nitrides, QSCE may simply be suppressed by switching to the metastable cubic zinc-blende structure.

F. Meier, M. Littmann, J. Bürger, T. Riedl, D. Kool, J. Lindner, D. Reuter, D. J. As
Department of Physics
University of Paderborn
Warburger Straße 100, 33098 Paderborn, Germany
E-mail: fmeier5@mail.upb.de; d.as@uni-paderborn.de

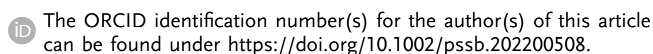
The ORCID identification number(s) for the author(s) of this article can be found under https://doi.org/10.1002/pssb.202200508.

© 2022 The Authors. physica status solidi (b) basic solid state physics published by Wiley-VCH GmbH. This is an open access article under the terms of the Creative Commons Attribution-NonCommercial License, which permits use, distribution and reproduction in any medium, provided the original work is properly cited and is not used for commercial purposes.

DOI: 10.1002/pssb.202200508

Cubic group III nitrides already received some attention among different research groups. Epitaxial growth of cubic gallium nitride (c-GaN) was conducted on different substrates with a suitable (zinc-blende) structure, e.g., Si, GaAs, MgO, and 3C-SiC.[5] However, the minimal lattice mismatch is 3.2% for c-GaN/3C-SiC (001). While the cubic phase can be epitaxially purported, overcoming metastability, the crystal quality (dislocation density, surface roughness) is very limited due to lattice mismatch.

Several ways to compensate for the mismatch are described in the literature[6–11] for zinc-blende material systems. Mismatch in such systems can be compensated by phase transitions of merging growth fronts,[6,7] aspect ratio trapping (ART),[9,10] nano-heteroepitaxy (NHE),[8] epitaxial lateral overgrowth (ELO),[11] and more.

Liu and Bayram et al.[6,7] revealed that if two hexagonal GaN growth fronts merge with a tetrahedron bonding angle of 109.47°, cubic GaN via a wurtzite to the cubic phase transition is formed on (111) faceted Si (001) substrate. The work of Kemper[8] revealed defect-free c-GaN nucleation on (111) facets of 3C-SiC (001). Reproducing this on purpose with pre-patterned substrates and proper selective area growth (SAG) could result in fewer defective c-GaN layers after coalescence.

ART[9] was shown to be a very potent technique for reducing dislocation densities. Smooth surfaces after the coalescence of GaAs were shown by Hsu et al.[10] for selective growth on Si covered with SiO_2 growth masks. The geometrical aspect ratio between mask opening and mask thickness can be designed in a way that stacking faults (SFs) terminate on the SiO_2 sidewalls. This process is called trapping as the SFs cannot propagate out of the growth mask. For gallium nitride, with ≈54.7° SF, such masks would require an aspect ratio of 1.4 at least.

Besides the work of Kemper,[8] all of the mentioned techniques were performed in metal–organic chemical vapor deposition (MOCVD) setups, where selectivity could be achieved by just offering <001> and <111> facets. In our plasma-assisted molecular beam epitaxy (PAMBE) setup, this requires a growth mask and parameters (e.g., III/V flux ratio, substrate temperature) optimized for selective deposition.

SAG of cubic gallium nitride (c-GaN) by PAMBE was first reported by Meier et al.[12] in macroscopic mask openings, employing SiO_2 as a growth mask. To research ART, ELO,

and phase transition techniques on c-GaN, selectivity has to be achieved on nanoscopic patterns. In addition, coalescence has to be achieved after nano-selective nucleation. If SAG of c-GaN is possible on nanoscales, crystal quality could be improved when growing c-GaN on 3C-SiC (001) by PAMBE, utilizing the aforementioned techniques.

Recently, a model for SAG of h-GaN has been proposed by Gridchin et al.[13] that also fits our observations qualitatively. It postulates that, within certain ranges, different growth regimes can be described by III/V flux ratios versus substrate temperature. For high substrate temperatures and small III/V flux ratios, no growth occurs because the residence time of Ga is too small for nucleation. If it is vice versa, growth happens on all surfaces and is not selective. From substrate temperatures of 775 °C to over 900 °C, they postulate a range of III/V flux ratios for every substrate temperature actually resulting in SAG of GaN.

The growth mechanism of c-GaN at such high temperatures in PAMBE setups is still subject to current research. Nevertheless, such growth temperatures were reported to result in high cubic phase contents in MOCVD setups.[14] This work is meant to prove the concept of nano-SAG by deposition of c-GaN in different structures.

2. Experimental Section

Within this section, the utilized substrates, the deposition, and the structuring of SiO_2 as well as c-GaN growth will be discussed briefly. For the deposition of mask materials physical vapor deposition (PVD), plasma-enhanced chemical vapor deposition (PECVD), and thermal oxidation were applied. Lithographic techniques, like nanosphere lithography (NSL), block co-polymer lithography (BCP), and electron beam lithography (EBL) were employed for structuring. Reactive ion etching (RIE) processes were utilized for etching the 3C-SiC/Si (001) pseudo substrates and SiO_2 masks. The section is concluded with a description of GaN deposition within our PAMBE setup and a rough description of transmission electron microscopy (TEM) specimen preparation.

3C-SiC/Si (001) substrates were supplied by NovaSic[15] and 3C-SiC/Si (001) with 4° miscut toward [110] were supplied by Kubos.[16] 200 nm thick films of SiO_2 were employed to achieve growth masks for PAMBE of GaN.

Plasma deposition of (P-)SiO_2 was done in an Oxford Plasmalab 80 PECVD apparatus. P-SiO_2 was grown at a rate of 73 nm min^{-1} at 300 °C. The plasma was operated at 20 W, 1000 mTorr, and supplied with 400 SCCM of SiH_4 and N_2O.

Thermal oxides (T-SiO_2) were also employed. As reported, plasma-deposited masks yielded a difference in substrate temperatures necessary for SAG of GaN of about 40 °C.[12] Besides different substrate and mask roughnesses after processing, the thermally oxidized substrates formed an oxide on all surfaces whereas P-SiO_2 is only deposited on the front side of the wafer. After deposition of 200 nm of T-SiO_2 on the SiC-side of 3C-SiC/Si (001), about 1.5 μm of T-SiO_2 was observed on the Si-side of the 3C-SiC/Si (001), resulting in a perfect mirror for thermal radiation. This could explain the significant change in substrate behavior while conducting SAG with T-SiO_2. As a consequence, this work will mainly focus on P-SiO_2. All samples were treated with acetone and isopropanol before and after the deposition of SiO_2.

Patterning of larger areas ($A > 2 \times 2\, cm^2$) was done by NSL and BCP.[17–19] Resulting masks consisted of hexagonally close-packed holes. The processes were designed to yield nominal hole diameters of 130 nm (NSL) and 17 nm (BCP). EBL was used to write grooves with a nominal width of 100 nm and length of 1 mm. The grooves were separated by SiO_2 barriers, designed to be 150 nm thick.

NSL utilized polystyrene spheres with a diameter of 200 nm that can be deposited in monolayers. Deposition was done by convective self-assembly by doctor blading, leading to a hexagonal close-packed monolayer of spheres.[17] Subsequently, the spheres were shrunk from 200 nm to 130 nm in diameter by an RIE step with Ar/O_2 chemistry. The shrunk spheres were then covered with 12.5 nm of nickel by PVD and removed with toluene in a supersonic bath. The remaining nickel layer with holes serves as a hard mask for the RIE of SiO_2. Afterward, nickel was removed by diluted H_2SO_4 in a supersonic bath.

Experimental details on the fabrication of a BCP mask can be found in ref. [17]. BCP employed a mixture of poly(styrene-b-methyl methacrylate) (PS-b-PMMA) that is spin-coated onto the substrate. The following annealing above the glass transition temperature generated microphase separation leading to PMMA cylinders in a PS matrix. The PMMA was then selectively removed, leaving the PS matrix that serves as a hard mask for the RIE of P-SiO_2. Subsequently, the PS matrix was removed by diluted H_2SO_5 in a supersonic bath.

Patterning of V-shaped grooves was achieved by e-beam lithography EBL in a Raith Pioneer field emission scanning electron microscope. Samples were spin-coated with Zeon Corporation ZEP520A[20] resist at 5500 rpm followed by a bake at 180 °C for 150 s. Patterning was done with a dose of 75 μC cm^{-2}. For every 10 grooves, the photo-resist mask needed a 500 nm barrier (spacer) for stabilization. To achieve V-shaped grooves in 3C-SiC, a subsequent SF_6 RIE step was employed, using the SiO_2 as a hard mask for RIE. Development of the EBL resist was done in n-amyl acetate, followed by isopropyl alcohol and deionized water rinse. The patterned EBL resist was then used as a hard mask for SiO_2 and the subsequent SF_6 RIE. ZEP520A was removed by hot acetone in a supersonic bath. All three lithography methods require careful optimization in terms of hard mask deposition parameters, RIE parameters, and wet chemical selective etching of hard masks. A special challenge is a circumstance, that it was not possible to remove the BCP and EBL resists in an oxygen plasma as usually employed, because this oxidizes uncovered 3C-SiC, rendering the substrate unusable. Results of the optimized and final patterns are shown in **Figure 1** and discussed in the results section.

SiO_2 RIE was done in an Oxford Plasmalab 100, operated at 25 W, 30 mTorr, and fed with 20 SCCM of each, CHF_3 and Ar. SF_6 RIE was also done in an Oxford Plasmalab 100 but was operated at 100 W, 95 mTorr, and supplied with 100 SCCM of SF_6.

After another acetone, isopropyl alcohol, and deionized water rinse, the patterned samples were introduced into the ultra high vacuum (UHV) of our PAMBE. Parameters for SAG were estimated with substrate temperatures ranging from 870 to 955 °C. Gallium beam equivalent pressures (BEP) were varied

© 2022 The Authors. physica status solidi (b) basic solid state physics published by Wiley-VCH GmbH
15213951, 2023, 8, Downloaded from https://onlinelibrary.wiley.com/doi/10.1002/pssb.202200508 by Univ/Bibliothek Paderborn, Wiley Online Library on [15/08/2023]. See the Terms and Conditions (https://onlinelibrary.wiley.com/terms-and-conditions) on Wiley Online Library for rules of use; OA articles are governed by the applicable Creative Commons License

15213951, 2023, 8, Downloaded from https://onlinelibrary.wiley.com/doi/10.1002/pssb.202200508 by Univ/Bibliothek Paderborn, Wiley Online Library on [15/08/2023]. See the Terms and Conditions (https://onlinelibrary.wiley.com/terms-and-conditions) on Wiley Online Library for rules of use; OA articles are governed by the applicable Creative Commons License

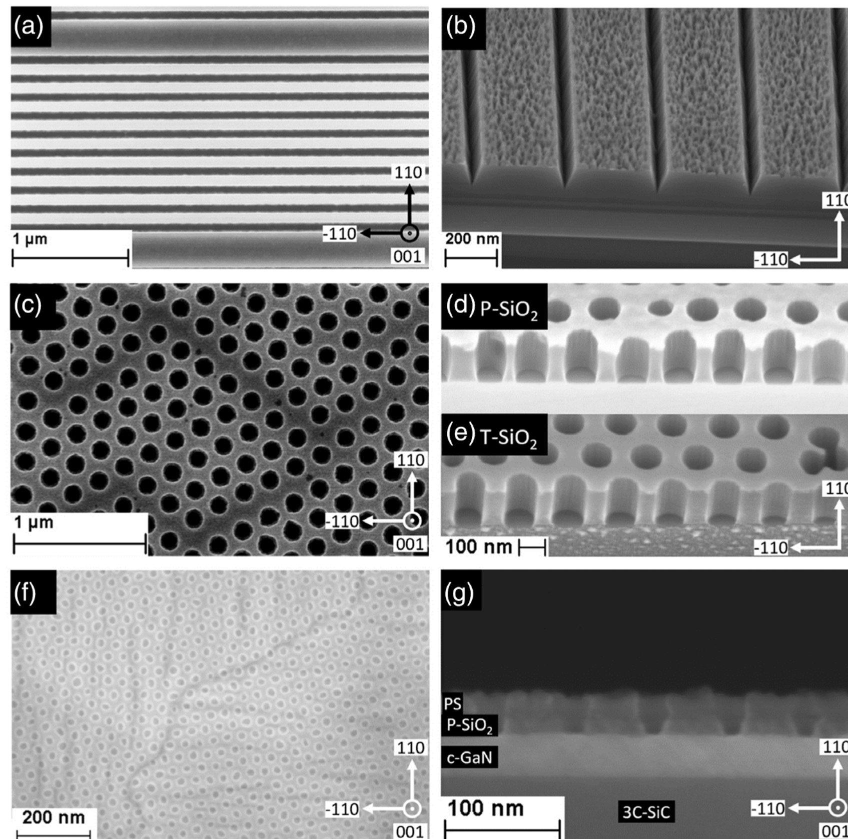

Figure 1. Scanning electron microscope (SEM) images of employed SiO_2 masks. a) Top-down view of grooves etched into P-SiO_2, electron beam lithography (EBL) resist already removed. b) 45° tilted view of cleaved V-shaped grooves in 3C-SiC after SF_6 reactive ion etching (RIE). c) Top-down view of nanosphere lithography (NSL) mask transferred into T-SiO_2 by RIE, with nickel already removed. d,e) 45° tilted view of a cleaved NSL masks etched into: (d) P-SiO_2 and (e) T-SiO_2, nickel already removed. f) Top-down view of a block co-polymer lithography (BCP) mask transferred into 20 nm of P-SiO_2, PS mask already removed. The c-GaN buffer layer is visible through the P-SiO_2 mask. g) Side-view of a cleaved BCP mask etched into P-SiO_2 with PS still on top.

from 6.5×10^{-8} to 2.9×10^{-6}mbar. At regular growth conditions, at a substrate temperature of around 720 °C, described by Lischka et al.,[5] Ga flux is $\approx 2 \times 10^{14}$ Atoms $[\text{cm}^2\text{s}]^{-1}$ at a Ga BEP of about 10^{-7}mbar. Growth was conducted for 3 h in most cases.

While NSL masks served for parameter search, grooves were employed to see if c-GaN can be deposited onto the <111> facets of 3C-SiC without the formation of hexagonal interlayers or inclusions. BCP masks were employed to test if coalescence is possible after NSAG. All masks were also meant to prove the possibility of SAG on the nanoscale with the smallest nominal feature size of 20 nm (BCP). BCP was tested heteroepitaxially on 3C-SiC (001) and homoepitaxially on a 40 nm c-GaN (001) buffer on 3C-SiC.

Post-growth characterization was done by means of TEM in a JEOL JEM-ARM200F at 200 kV, TEM bright field on a 4 k × 4 k CMOS camera (Gatan OneView) without any contrast enhancing objective lens aperture. TEM samples were conventionally prepared with cross-section mechanical dimple grinding followed by an ion milling step in a GATAN PIPS.

Surface morphologies were imaged by the same Raith Pioneer field emission scanning electron microscope used for EBL. For imaging, it is operated at 5 kV and detects backscattered electrons by the "Gemini in-lens" detector.

Furthermore, high-resolution X-ray diffraction (HRXRD) was conducted in a Malvern X'Pert device, using a copper anode operated at 40 mA and 45 kV. Especially the very small deposited volumes made both techniques very challenging. For HRXRD everything but the structure was either masked with lead tape or cleaved out.

3. Results and Discussion

The results will be discussed with respect to the employed mask structure. At first, an overview of the achieved patterns is given to show what structures were tinkered with and utilized in this work. To confirm crystallographic phases from TEM images on nanoscopic scales, theoretical and real images of the wurtzite and zinc blende lattice as well as their fast Fourier transforms (FFTs) are compared. The following three subsections depict and discuss the results from the overgrowth of NSL, EBL, and BCP patterned 3C-SiC and SiO_2. As NSL allows the patterning of large areas within a reasonable time, it was mainly employed

© 2022 The Authors. physica status solidi (b) basic solid state physics published by Wiley-VCH GmbH

15213951, 2023, 8, Downloaded from https://onlinelibrary.wiley.com/doi/10.1002/pssb.202200508 by Univ/Bibliothek Paderborn, Wiley Online Library on [15/08/2023]. See the Terms and Conditions (https://onlinelibrary.wiley.com/terms-and-conditions) on Wiley Online Library for rules of use; OA articles are governed by the applicable Creative Commons License

to probe for parameters leading to SAG on partially masked 3C-SiC (001) surfaces. EBL was used for the patterning of V-shaped grooves. Such grooves approximately expose <111> facets of 3C-SiC, and therefore allow to test NSAG on 3C-SiC (111). The experiments were concluded by reducing the structure sizes of about one order of magnitude by utilizing a BCP process, yielding hole diameters of 17 nm instead of the 130 nm achieved by NSL.

Figure 1 shows the results of SiO_2 patterning by SEM imaging. Figure 1a shows grooves with vertical sidewalls in SiO_2 on a 3C-SiC/Si (001) substrate. EBL resist was removed with acetone and the mask fulfilled the aforementioned nominal dimensions. A subsequent SF_6 RIE process transferred the grooves into 3C-SiC with an anisotropic etch approximately dissecting <111> facets along [110] as shown in Figure 1b. Performing RIE without removing EBL resist beforehand results in smoother SiO_2 surfaces. Nevertheless, structuring V-shaped grooves always leaves the SiO_2 mask damaged as the EBL resist is not resistant enough to withstand SF_6 RIE.

NSL patterned structures on thermal and plasma-deposited silicon oxides can be seen in Figure 1c–e. Structuring with NSL worked as described in the Experimental Section, creating mask openings with a diameter of 130 nm and a depth of 200 nm. Sidewalls look steep and the etching is selective with negligible over-etching into the substrate. Also, the SiO_2 surface is completely protected by the Ni-hard mask.

BCP lithography was conducted on a 20 nm P-SiO_2 film deposited on 40 nm of c-GaN. Figure 1f depicts the BCP patterned P-SiO_2 after processing in the top-down view. Besides the 17 nm openings, the c-GaN buffer morphology is visible through the 20 nm thick P-SiO_2 mask. Figure 1g shows a side-view of the BCP patterned P-SiO_2 mask after RIE processing. Dimensions were estimated from the SEM images. Before depositing P-SiO_2 the c-GaN surface exhibited a root mean square roughness of 1 nm on a $10 \times 10\,\mu m^2$ area measured by atomic force microscopy (AFM). The aspect ratio of 1 was chosen as the geometrical arrangement of evaporation cells and substrate is limiting the Ga flux to reach the bottom of holes with an aspect ratio greater than 1.8. Besides that, the focus of implementing the BCP process was to experimentally verify the possibility of coalescence after NSAG of GaN.

On nanoscopic scales, the GaN phase had to be verified by the FFT of the TEM images. **Figure 2** gives an idea of how to interpret the TEM images and the FFT patterns obtained from them.

Figure 2a shows the zinc blende unit cell and its projection toward [110] zone axis orientation with a ball and stick theme plotted with Vesta.[21] Figure 2b depicts a bright field TEM measurement of the real lattice which matches the reorientated ball and stick theme. Figure 2c,d shows FFTs of simulated and TEM measured c-GaN, respectively. Simulation of FFT was done by Carine.[22] If the FFT pattern resembles a parallelogram, with equidistant reflexes, a cubic phase can be assumed.

3.1. GaN Growth on NSL Mask Patterned 3C-SiC (001)

NSAG was carried out on NSL patterned SiO_2 masks on 3C-SiC (001) substrates first. It was possible to achieve nanoselective growth on plasma deposited and thermal silicon oxides. The first striking insight is that selective growth can be achieved within a large range of substrate temperature and III/V flux ratio pairs,

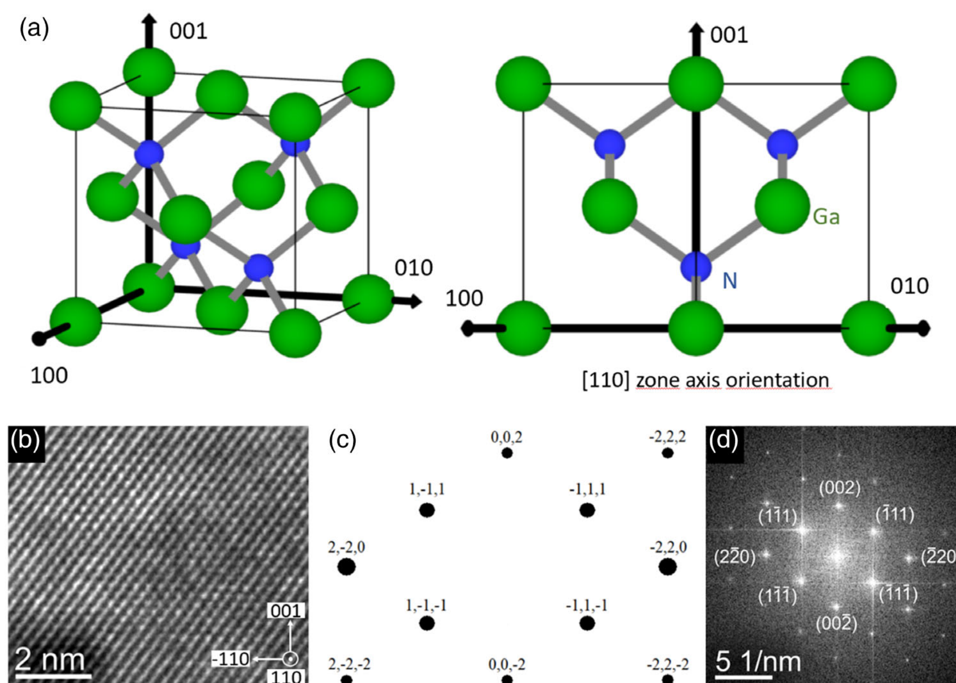

Figure 2. a) Vesta drawing of the zinc blende unit cell of GaN and zone axis orientation toward [110]. b) transmission electron microscope (TEM) bright field image of the real c-GaN lattice. c) Carine fast Fourier transform (FFT) simulation of the simulated and reorientated unit cell. d) FFT of the TEM bright field image, confirming cubic phase.

© 2022 The Authors. physica status solidi (b) basic solid state physics published by Wiley-VCH GmbH

15213951, 2023, 8, Downloaded from https://onlinelibrary.wiley.com/doi/10.1002/pssb.202200508 by Univ/Bibliothek Paderborn, Wiley Online Library on [15/08/2023]. See the Terms and Conditions (https://onlinelibrary.wiley.com/terms-and-conditions) on Wiley Online Library for rules of use; OA articles are governed by the applicable Creative Commons License

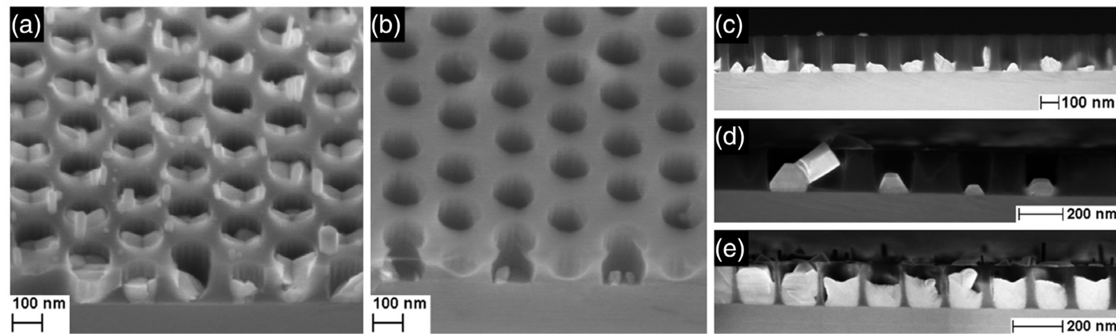

Figure 3. Angled- and side-view SEM images of different overgrown NSL patterned SiO_2 masks. All samples were overgrown for 3 h. a,b) T-SiO_2 NSL pattern overgrown at a substrate temperature of 890 °C: (a) was overgrown with a Ga BEP of 6.9×10^{-7} mbar and (b) was overgrown with a Ga BEP of 3.7×10^{-7} mbar. c–e) Overgrown P-SiO_2 NSL masks: (c) was overgrown at 870 °C with a Ga BEP of 6.5×10^{-8} mbar, (d,e) were overgrown at 935 °C with a Ga BEP of 3.7×10^{-7} mbar.

opening a big parameter space as also described by Gridchin et al.[13] To emphasize this, **Figure 3** shows NSAG for substrate temperatures of 870, 890, and 935 °C on NSL-structured SiO_2 masks. Figure 3a,b shows overgrown T-SiO_2 masks and Figure 3c–e shows overgrown P-SiO_2 masks. To achieve selective growth, either the substrate temperature or the III/V flux ratio has to be fixed. However, the growth rate is strongly coupled to selectivity and it was not possible to achieve growth rates above 80 nm h^{-1} while maintaining good selectivity. Dividing the grain sizes along [001] by the total deposition time of 3 h approximates the total growth rate. This assumption neglects the fact that the growth rates of forming nuclei (nucleation) and quasi-2D island growth (steady state) mode deviate.[23] Samples with good selectivity grow extremely slow (compare Figure 3a,b). Both depicted samples were overgrown for 3 h. In case of Figure 3b, the total growth rate was below 10 nm h^{-1}. It is unclear to what extend both growth regimes are influenced by selective growth. As the SAG process can be modeled by nucleation rates[13] it is thinkable that the total growth rate is lowered by delayed nucleation of GaN. Once nucleated, the steady-,state growth rate could remain unchanged. To properly address this question, the nucleation process at such high temperatures has to be researched further.

The morphology of selectively grown GaN crystals within holes is somehow randomly distributed. A lot of holes are filled by grains with a characteristic V-shape (see Figure 3a). This can be attributed to the rotation of the sample (see Section 3.2). The other holes are either filled with single- or multi-domain grains. The holes are large enough for more than one nucleus (see Figure 3b). If multiple nuclei coalesce, defects can be introduced and growth is perturbed, leading to different grains within every hole (see Figure 3c). In case of a single grain, growth happens dominantly along <111> facets (see Figure 3d). While such a grain is still cubic, <111> facets of c-GaN are known to have a good chance of undergoing a zinc blende to the wurtzite phase transition.

When samples rotate the impinging flux III/V ratio on each <111> facet oscillates. This causes the growth to oscillate between metal and nitrogen rich. Excess nitrogen promotes the formation of hexagonal inclusions.[5,24] Figure 3d shows how a hexagonal [0001] GaN rod emerged from a [111] facet of the c-GaN grain. If this happens in both directions, the characteristic V-shape is formed. The V-shape is probably a result of crystal twinning introduced by rotation. In the case of Figure 3c,d the grains grow flat to some extent. It is not clear, how to precisely control morphology when conducting NSAG, yet. An important step for morphology control would be homogeneous nucleation. Thin GaN or aluminum nitride (AlN) buffer layers, below the SiO_2 masks, could help to achieve homogeneous nucleation when conducting SAG.

Nevertheless, if the characteristic V-shape does not occur, grains seem to grow in the zinc blende phase with stacking faults (SFs) along the <111> facets. **Figure 4** shows such a grain, depicted by a cross-section bright field TEM image. The horizontal pattern across the grain is a result of TEM preparation. SF are forming on both, the c-GaN/3C-SiC and

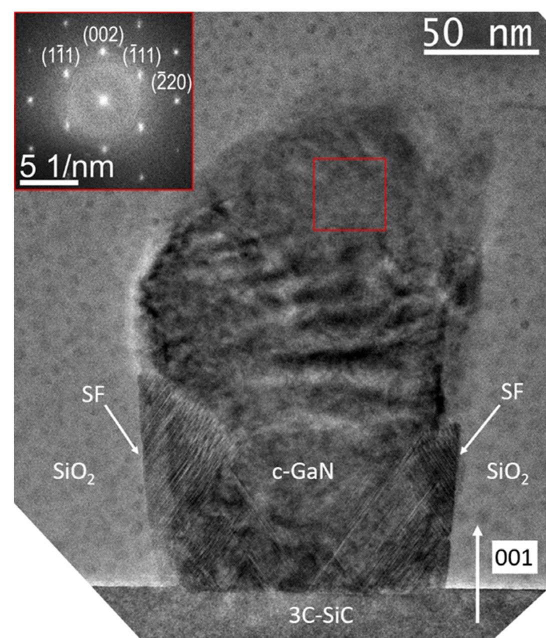

Figure 4. Rotated TEM cross-section bright field image of a selectively grown GaN grain within an opening of a P-SiO_2 mask. FFT inset (red box) suggests phase pure cubic GaN.

© 2022 The Authors. physica status solidi (b) basic solid state physics published by Wiley-VCH GmbH

c-GaN/SiO_2 interfaces. It looks like SF disappear somehow without annihilation. SF termination, and therefore ART was difficult to show, yet. SF form mostly in the vicinity of the sidewalls of the holes. On the top part of the grain, however, approaching the mask opening, phase pure cubic GaN was observed as can be seen by the FFT inset in Figure 4. No SF is observable in the top part of the grain.

3.2. GaN Growth on V-Shaped Groove Patterned 3C-SiC (001)

As observed by Kemper,[8] c-GaN can be grown in V-shaped 3C-SiC grooves approximately exposing <111> facets along [110] without hexagonal interlayers. Previous works were not doing this selectively. As proper parameters were estimated by Meier et al.[12] we were able to reproduce this purposefully and selectively.

Figure 5 shows SEM and TEM images of a sample overgrown at 935 °C with Ga BEP of $2.9{\cdot}10^{-6}$ mbar. To achieve nucleation on 3C-SiC surfaces, approximately dissecting <111> facets, a higher III/V flux ratio was necessary compared to NSAG on 3C-SiC (001). Increasing the Ga flux resulted in the good filling of grooves. The grains expose the typical V-shape that was already observed when overgrowing holes patterned by NSL. The side view of the grooves shows three domains within the grains (see red dashed lines). Figure 5a,b shows TEM measurements and their FFT from the grooves' tip and the intersection of the grain boundaries.

Nearly defect-free cubic GaN can be observed within the tip. This is also confirmed by the FFTs given in the insets. At the grain boundary intersection, a c-GaN(111)/h-GaN(0001) transition can be observed. The (111)/(0001) interface of the phase transition seems to intersect with the 3C-SiC/SiO_2 interface. FFTs of the areas next to the grain boundaries reveal hexagonal GaN (see Figure 5c). Beyond the cubic to the hexagonal phase transition, GaN continues to grow as a hexagonal twin. Crystal twins form the V-shape that has already been observed when overgrowing NSL masks. Again, this is caused by sample rotation. When overgrowing grooves, this can be avoided by precisely aligning the substrate with respect to the gallium cell and growing without rotation. The Ga flux vector projection onto the samples surface has to be parallel to the grooves. Figure 5 clearly shows that it is possible to have c-GaN purposefully nucleate on <111> facets of 3C-SiC in V-shaped grooves along [110], verified by TEM imaging.

Figure 6 shows SEM images of another sample, grown at 955 °C with a Ga BEP of $3.2{\cdot}10^{-6}$ mbar and without rotation for 3 h. For the substrate temperature of 935 °C, the growth was not selective (see Figure 5). For that reason, the substrate temperature was increased to restore selectivity. The substrate was carefully aligned to have the Ga beam irradiate the tips of the grooves. This was achieved by orientating the substrate with respect to the Ga cell by macroscopic marks scribed into the sample before conducting EBL. Grooves are then orientated with respect to the scribing marks. The marks themselves are visible after introducing the sample into the PAMBE setup. By aligning the scribing marks toward the Ga cell, one also aligns the grooves. Together these measures restored selectivity and led to the controlled filling of the grooves without any obvious

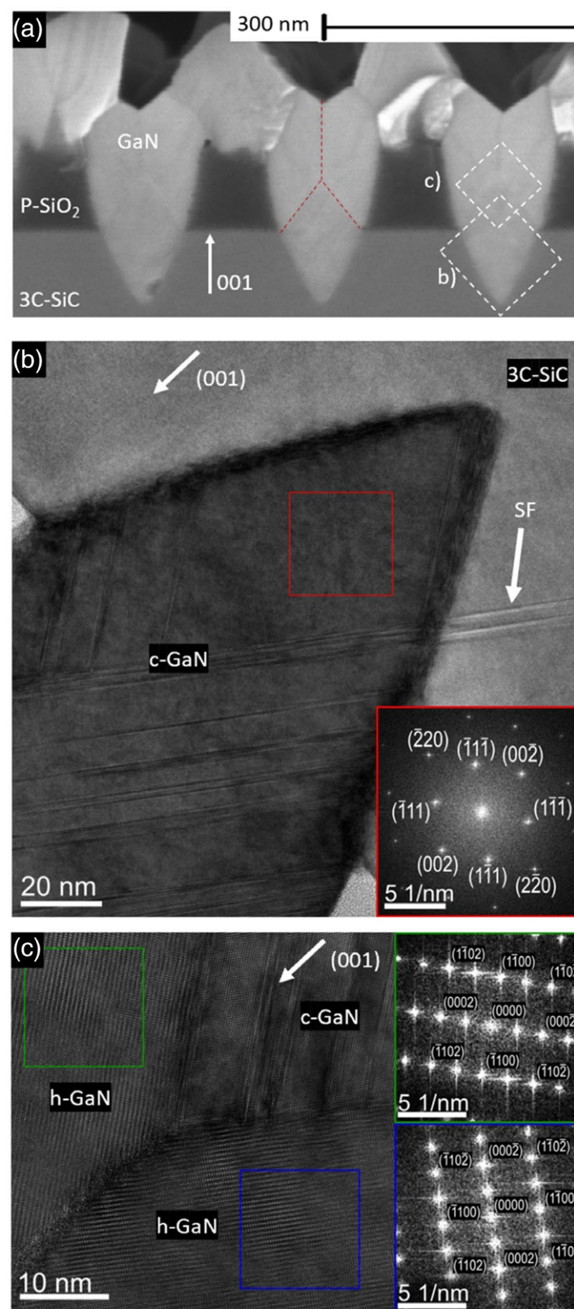

Figure 5. SEM and TEM images of overgrown V-shaped grooves in 3C-SiC. a) SEM side-view showing grooves filled with GaN in masked 3C-SiC. b) TEM image of the tip region confirming phase pure c-GaN. c) TEM image of the grain boundary intersection showing a cubic to hexagonal phase transition, forming a hexagonal twin. Phases were identified by FFT insets.

hexagonal inclusions. Furthermore, this observation proves that the origin of V-shaped grains is the rotation of the sample and that V-shapes are the results of crystal twinning.

Figure 6 left shows the top-down SEM view of 10 overgrown grooves. At this stage, different surface morphologies emerge with a boundary. From the micrometer scale of the boundary, such domains are suspected to correspond to the anti-phase

© 2022 The Authors. physica status solidi (b) basic solid state physics published by Wiley-VCH GmbH

15213951, 2023, 8, Downloaded from https://onlinelibrary.wiley.com/doi/10.1002/pssb.202200508 by Univ/Bibliothek Paderborn, Wiley Online Library on [15/08/2023]. See the Terms and Conditions (https://onlinelibrary.wiley.com/terms-and-conditions) on Wiley Online Library for rules of use; OA articles are governed by the applicable Creative Commons License

15213951, 2023, 8, Downloaded from https://onlinelibrary.wiley.com/doi/10.1002/pssb.202200508 by Univ/Bibliothek Paderborn, Wiley Online Library on [15/08/2023]. See the Terms and Conditions (https://onlinelibrary.wiley.com/terms-and-conditions) on Wiley Online Library for rules of use; OA articles are governed by the applicable Creative Commons License

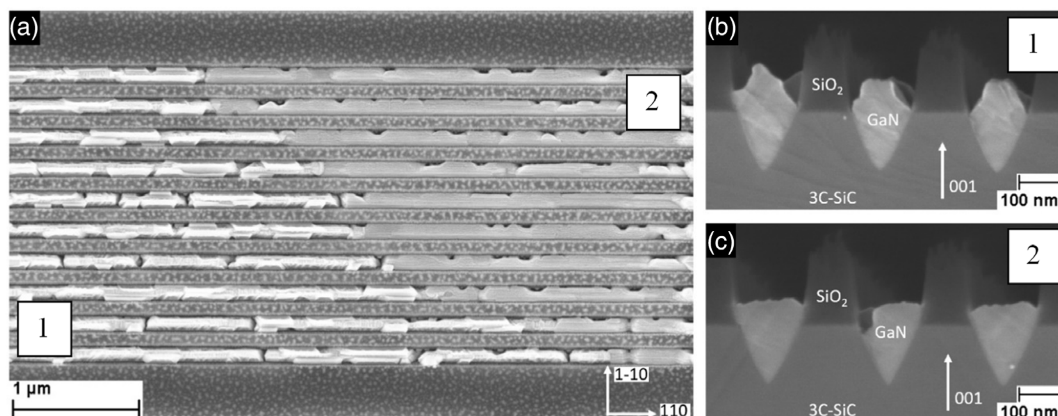

Figure 6. SEM images of selectively overgrown V-shaped grooves. a) Top-down view of the grooves. Anti-phase domains (APDs) cause different morphologies (markers 1 and 2) of the grown GaN. b) Side-view along domain 1. c) Side-view along domain 2. Overgrowth was done at 955 °C with a Ga beam equivalent pressure (BEP) of 3.2×10^{-6} mbar.

domain (APD) of the 3C-SiC substrate. Both domains are marked with 1 or 2.

Figure 6 right shows side-view SEM images of three cleaved grooves with respect to each domain. For both domains, the grooves have been filled bottom up. No grain boundaries can be seen in the side view. To estimate cubic phase content HRXRD was conducted. Reciprocal space maps (RSMs) of the 002 Reflex along both main azimuths allow to estimate the hexagonal fraction by comparing integral intensities of cubic and hexagonal reflections.[25] The sample shown in Figure 6 exhibits a hexagonal phase fraction of 44%.

APDs, originating from the 3C-SiC substrate, can be avoided by employing miscut substrates.[26] APDs form when growing 3C-SiC on Si because of monoatomic steps.[27] By employing miscut Si, the formation of APDs is already suppressed during 3C-SiC growth and therefore cannot influence GaN epilayers. To prove that observed domains correspond to APDs and to further optimize the homogeneity of nanoselectively grown GaN in V-shaped grooves, 4° miscut 3C-SiC substrates, with the miscut aligned towards [110], were employed.

Figure 7 shows SEM images of two samples overgrown at 950 °C with Ga BEP of 3.6×10^{-6} mbar and without rotation for 3 h. Grooves were orientated parallel with respect to the 4° miscut towards [110]. Red arrows indicate the direction of the miscut. It can be seen from the comparison that the formation of domains may be overcome by the implementation of miscut substrates. Earlier experiments in our PAMBE setup also revealed that no APDs form when GaN is grown on unpatterned miscut 3C-SiC. Here it was possible to mimic both morphologies (Figure 6 1,2) by just aligning the grooves parallel (Figure 7b) and perpendicular (Figure 7a) to the miscut. When the grooves are perpendicular and parallel to miscut the morphology resembles

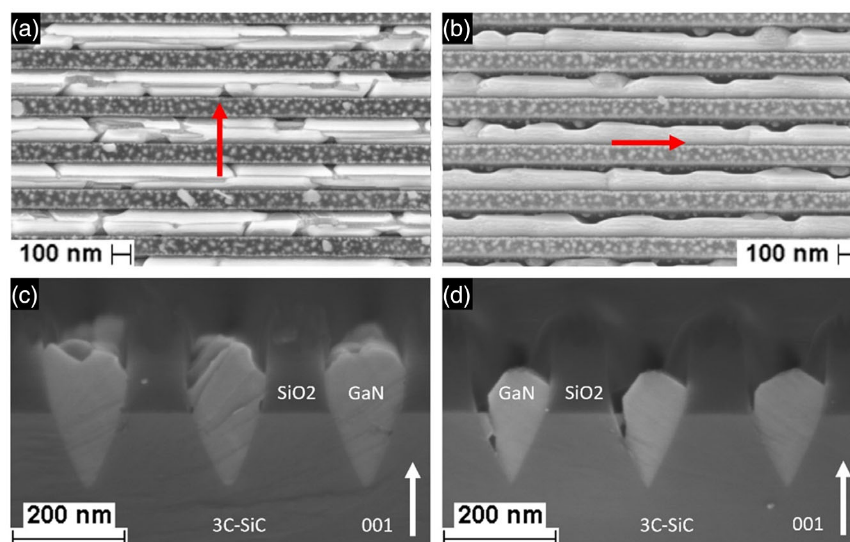

Figure 7. SEM images of two selectively overgrown samples of V-shaped grooves in miscut 3C-SiC. Miscut is orientated toward [110] and its direction is indicated by a red arrow for each sample. a,c) Top-down and side-view of overgrown grooves perpendicular to miscut (h-GaN content ≈18%). b,d) Top-down and side-view of overgrown grooves parallel to miscut (h-GaN content ≈95%).

 © 2022 The Authors. physica status solidi (b) basic solid state physics published by Wiley-VCH GmbH

15213951, 2023, 8, Downloaded from https://onlinelibrary.wiley.com/doi/10.1002/pssb.202200508 by Univ/Bibliothek Paderborn, Wiley Online Library on [15/08/2023]. See the Terms and Conditions (https://onlinelibrary.wiley.com/terms-and-conditions) on Wiley Online Library for rules of use; OA articles are governed by the applicable Creative Commons License

domains 1 and 2 of the previous sample, respectively. This also prooves that the domains really correspond to the APD's of the 3C-SiC substrate.

RSM of the 002 reflexes along both main azimuths implies very different phase contents dependent on the chosen groove orientation with respect to miscut. While GaN grown nanoselectively in grooves perpendicular to the miscut (see Figure 7 left) exhibits a hexagonal phase content of only 17.6%, selectively grown GaN in grooves parallel to the miscut (see Figure 7 right) yielded a hexagonal content of ≈95%. When the grooves are parallel to miscut the grown GaN grains look very smooth but

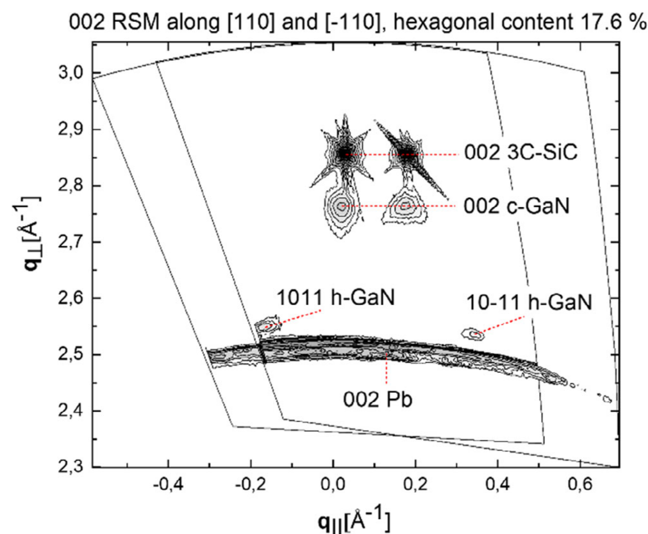

Figure 8. Reciprocal space map (RSM) of selectively overgrown V-shaped grooves orientated perpendicular toward the [110] miscut direction of the 3C-SiC/Si (001) substrate (Figure 7 left). By calculating the ratio of integral intensities for the visible GaN reflexes, hexagonal content was estimated to be 17.6%.[25]

are hexagonal. For grooves perpendicular to miscut, the lowest hexagonal content was achieved, yet.

Figure 8 shows the RSMs along both main azimuths for the sample with grooves perpendicular (Figure 7a) to the miscut. As the substrate is miscut 4° toward [110], it is possible to plot both RSMs within one graph. Besides the strong 3C-SiC (002) reflection, c-GaN (002) reflections are visible, despite the tiny deposited volume.

Hexagonal GaN, grown on c-GaN facets, causes (10-11) and (1011) reflections. One can also see a preferred orientation of hexagonal inclusions. The Debye ring corresponds to Pb (002) which was used to cover everything but the structure. 17.6% of hexagonal inclusions was the best value achieved for growing c-GaN selectively into V-shaped grooves in 3C-SiC (001), yet. The hexagonal fraction of 17.6% may be significantly lowered by further optimization of growth parameters.

3.3. GaN Growth on BCP Mask Patterned 3C-SiC (001)

After demonstrating the possibility of nanoselective c-GaN growth on <001> and <111> surfaces of 3C-SiC, coalescence after selective nucleation is demonstrated, employing BCP patterning. This experiment was conducted homo- and heteroepitaxially at parameters found useful for the overgrowth of the V-shaped grooves. Thus, such parameters could be far from optimal.

Growth was conducted at a substrate temperature of 950 °C and a Ga BEP of 2.9×10^{-6} mbar for 2 h. **Figure 9** shows SEM images of the sample homoepitaxially overgrown, employing a c-GaN buffer. The top row shows the morphology of the sample's surface with increasing distance to the sample's center. The different morphologies are a result of a substrate temperature gradient. Approximately, this gives insight into different stages of growth.

Image (a) is from the sample's center (highest temperature), and shows selectively nucleated GaN with beginning

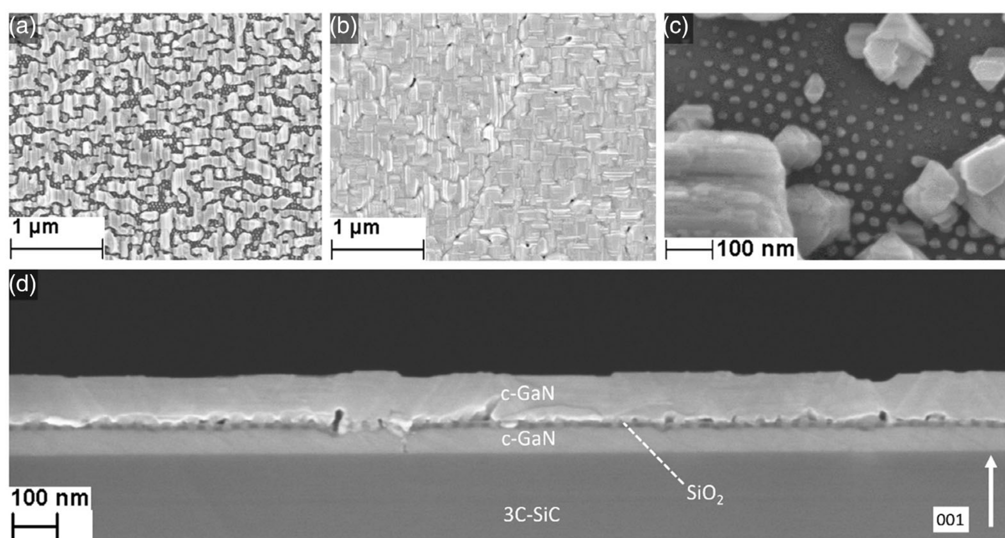

Figure 9. SEM images of a nanoselectively overgrown BCP P-SiO_2 mask covering a c-GaN buffer. a) Top-down view of the samples center after overgrowth. b) Top-down view 3 mm away from the samples center, exposing a closed film with cubic facets. c) Top-down view from the samples edge. Selectivity was not good enough to suppress parasitic nucleation but shows filled holes. d) Side-view of the coalesced GaN layer.

© 2022 The Authors. physica status solidi (b) basic solid state physics published by Wiley-VCH GmbH

15213951, 2023, 8, Downloaded from https://onlinelibrary.wiley.com/doi/10.1002/pssb.202200508 by Univ/Bibliothek Paderborn, Wiley Online Library on [15/08/2023]. See the Terms and Conditions (https://onlinelibrary.wiley.com/terms-and-conditions) on Wiley Online Library for rules of use; OA articles are governed by the applicable Creative Commons License

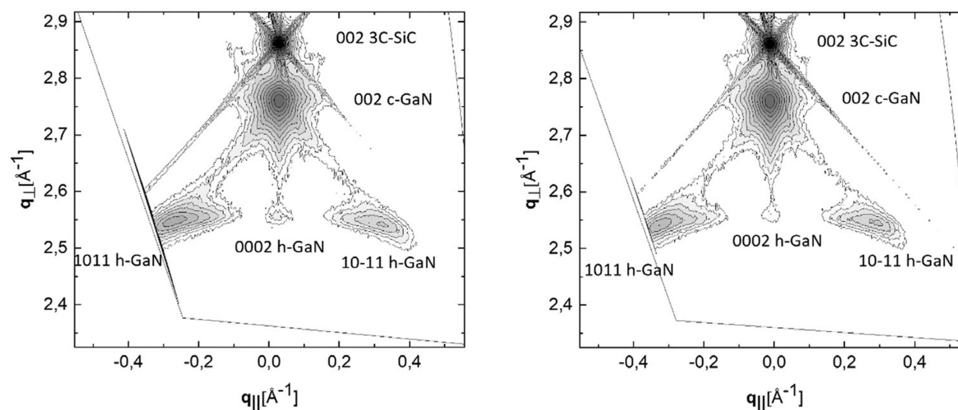

Figure 10. RSMs of the (002) reflections along both main azimuths. Hexagonal content was estimated to be ≈19%.[25]

coalescence. In between coalescing nuclei, it looks like the hole was filled selectively. However, grains grow at different speeds not resulting in a closed layer after 2 h of deposition. On coalesced grains, typical cubic facetation starts to emerge.

The top middle picture is about 3 mm away from the sample's center and indicates that a slightly lower substrate temperature results in faster nucleation, thus giving nuclei more time for coalescence. Even with some tiny gaps the layer looks closed and coalesced. It exhibits facets with a 90° angle in between, indicating a cubic phase.

The top right picture was taken from the vicinity of the edge of the sample (lowest temperature). The parasitic nuclei cast Ga shadows for the impinging beam, and therefore suppress the growth of grains in the nanoscopic openings. Nevertheless, it is clearly visible that the holes were selectively filled, thus confirming SAG on scales down to 17 nm all over the surface of the sample.

The large bottom picture depicts a side view along the coalesced layer (top middle picture). Besides underlining proper coalescence again, it shows that the facetation is caused by SFs propagating through the layer toward the surface.

Figure 10 shows the RSMs of the (002) reflections for the homoepitaxially grown sample. Hexagonal phase content was calculated to be 29% after taking the c-GaN buffer into account. Without subtracting the phase pure buffer, of about 40 nm thickness, hexagonal content is as low as 19%. The tilt of hexagonal reflexes could be a hint that we also measured the parasitically nucleated GaN on the SiO_2 mask, thus increasing the measured hexagonal content. In contrast, heteroepitaxial growth on masked 3C-SiC resulted in a layer thickness of 70 nm with a hexagonal content of about 44%. This reveals that a c-GaN buffer is beneficial for selective nucleation. Up to now we could not achieve reduced SF densities compared to c-GaN thin films grown on unmasked and unpatterned 3C-SiC (001). However, the presented results look promising.

4. Conclusion

In this work, we demonstrated the NSAG growth of cubic gallium nitride. We were able to deposit phase pure c-GaN grains in 130 nm NSL mask openings, confirmed by FFT of TEM bright-field images. Furthermore, defect-free nucleation of c-GaN on <111> facets of 3C-SiC/Si (001), inside V-shaped grooves, was shown by TEM. The best structural results on macroscopic scales ($1 \times 1\ mm^2$) were achieved by employing miscut substrates, suppressing APD formation. GaN grown in V-shaped grooves perpendicular to miscut exhibited a hexagonal phase content of 17.6%, estimated by HRXRD. Additionally, we found that the rotation of samples promotes the formation of hexagonal phase and twins on <111> facets of c-GaN and 3C-SiC. Finally, we were able to achieve c-GaN coalescence after NSAG on BCP masks. Growth in BCP masks confirms NSAG down to structure sizes of 17 nm and additionally shows that it is possible to achieve coalescence afterward, resulting in a cubic film. HRXRD revealed a hexagonal phase content of 29% after coalescence.

Together these results are very promising. After optimization of the structure processing and growth parameters, they could deliver an opportunity for the improvement of the structural quality of c-GaN to device qualities, overcoming the limits of lattice-mismatch-induced defects.

Acknowledgements

The authors gratefully acknowledge Cedrik Meier and his team for technical support in the deposition, patterning, and reactive ion etching of the different oxides and surfaces. Financial support was provided by Deutsche Forschungsgemeinschaft (DFG) to project As107/7-1 (Project no. 418748882).

Open Access funding enabled and organized by Projekt DEAL.

Conflict of Interest

The authors declare no conflict of interest.

Data Availability Statement

The data that support the findings of this study are available from the corresponding author upon reasonable request.

© 2022 The Authors. physica status solidi (b) basic solid state physics published by Wiley-VCH GmbH

Keywords

gallium nitride, nano selective area growth, plasma assisted molecular beam epitaxy, silicon carbide, zincblende

Received: October 26, 2022
Revised: December 15, 2022
Published online: December 29, 2022

[1] J. Huang, H. C. Kuo, S. C. Shen, *Nitride Semiconductor Light-Emitting Diodes (LEDs) Materials, Technologies and Applications*, Woodhead Publishing, UK, **2018**.
[2] O. Ambacher, M. S. Brandt, R. Dimitrov, T. Metzger, M. Stutzmann, R. A. Fischer, A. Miehr, A. Bergmaier, G. Dollinger, *J. Vac. Sci. Technol.* **1996**, *14*, 3532.
[3] S. Strite, H. Morkoç, *J. Vac. Sci. Technol.*, **1992**, *10*, 1237.
[4] V. Fiorentini, F. Bernardini, F. Della Sala, A. D. Carlo, P. Lugli, *Phys. Rev. B*, **1991**, *60*, 8849.
[5] K. Lischka, D. Schikora, D. J. As, in *Vacuum Science And Technology: Nitrides As Seen By The Technology*, Research Signpost, Kerala, **2002**.
[6] R. Liu, C. Bayram, *Appl. Phys. Lett.* **2016**, *109*, 042103.
[7] C. Bayram, J. A. Ott, K.-T. Shiu, C.-W. Cheng, Y. Zhu, J. Kim, M. Razeghi, D. K. Sadana, *Adv. Funct. Mater.* **2014**, *24*, 4492.
[8] R. Kemper, Ph.D. Thesis, *University of Paderborn,* **2014**.
[9] B. Kunert, W. Guo, Y. Mols, B. Tian, Z. Wang, Y. Shi, D. Van Thourhout, M. Pantouvaki, J. Van Campenhout, R. Langer, K. Barla, *Appl. Phys. Lett.* **2016**, *109*, 091101.
[10] C.-W. Hsu, Y.-F. Chen, Y.-K. Su, *Nanotechnology* **2012**, *23*, 495306.
[11] J. Wentao, D. A. Gulino, R. Higgins, *J. Cryst. Growth* **2004**, *263*, 30.
[12] F. Meier, M. Protte, E. Baron, M. Feneberg, R. Goldhahn, D. Reuter, D. J. As, *AIP Adv.* **2021**, *11*, 075013.
[13] V. O. Gridchin, L. N. Dvoretckaia, K. P. Kotlyar, R. R. Reznik, A. V. Parfeneva, A. S. Dragunova, N. V. Kryzhanovskaya, V. G. Dubrovskii, G. E. Cirlin, *Nanomaterials* **2022**, *12*, 2341.
[14] C. H. Wei, Z. Y. Xie, L. Y. Li, Q. M. Yu, J. H. Edgar, *J. Electron. Mater.* **2000**, *29*, 317.
[15] NOVASIC SA, Savoie Technolac, Le Bourget-du-Lac, France, https://www.novasic.com (accessed: October 2022).
[16] Kubos Semiconductors Ltd, Future Business Centre, Cambridge, UK, https://www.kubos-semi.com (accessed: October 2022).
[17] K. Brassat, D. Kool, J. Bürger, J. K. N. Lindner, *Nanoscale* **2018**, *10*, 10005.
[18] T. Riedl, V. Kunnathully, A. Karlisch, D. Reuter, J. K. N. Lindner, presented at *E-MRS Fall Meetin*, Warsaw, September 2017.
[19] T. Riedl, T. Langer, A. Trapp, J. Bürger, D. Reuter, J. K. N. Lindner, presented at *Euromat Congress*, Stockholm, September 2019, pp. PS1-6.
[20] Zeon Corporation, Data sheet EBL resist, https://www.zeon.co.jp/en/business/enterprise/electronic/imagelec/ (accessed: October 2022).
[21] K. Momma, F. Izumi, *J. Appl. Cryst.*, **2011**, *44*, 1272.
[22] C. Boudias, D. Monceau, Product description CaRine, http://carine.crystallography.pagesperso-orange.fr/WWW_FULL_DESCRIPT_CRYST.html (accessed: October 2022).
[23] R. L. Headrick, S. Kycia, Y. K. Park, *Phys. Rev. B* **1996**, *54*, 14686.
[24] D. Schikora, M. Hankeln, D. J. As, K. Lischka, *Phys. Rev. B* **1996**, *54*, R8381.
[25] M. Frentrup, L. Y. Lee, S.-L. Sahonta, M. J. Kappers, F. Massabuau, P. Gupta, R. A. Oliver, C. J. Humphreys, D. J. Wallis, *J. Phys. D: Appl. Phys.* **2017**, *50*, 433002.
[26] L. Y. Lee, M. Frentrup, M. J. Kappers, R. A. Oliver, C. J. Humphreys, D. J. Wallis, *J. Appl. Phys.* **2018**, *124*, 105302.
[27] J. Faucher, M. Taizo, M. L. Lee, *J. Vac. Sci. Technol. B* **2016**, *34*, 041203.

© 2022 The Authors. physica status solidi (b) basic solid state physics published by Wiley-VCH GmbH

15213951, 2023, 8, Downloaded from https://onlinelibrary.wiley.com/doi/10.1002/pssb.202200508 by Univ/Bibliothek Paderborn, Wiley Online Library on [15/08/2023]. See the Terms and Conditions (https://onlinelibrary.wiley.com/terms-and-conditions) on Wiley Online Library for rules of use; OA articles are governed by the applicable Creative Commons License